NANO LETTERS
Letter
Cite This: Nano Lett. 2018, 18, 2358−2364
pubs.acs.org/NanoLett

Coupling of Molecular Emitters and Plasmonic Cavities beyond the Point-Dipole Approximation

Tomáš Neuman,[†,‡] Ruben Esteban,[‡,§] David Casanova,[†,#,‡,§] Francisco J. García-Vidal,[‡,∥] and Javier Aizpurua*[,†,‡]

[†]Centro de Física de Materiales CFM-MPC (CSIC-UPV/EHU) and [#]Kimika Fakultatea, Euskal Herriko Unibertsitatea (UPV/EHU), 20018 San Sebastián-Donostia, Spain

[‡]Donostia International Physics Center (DIPC), 20018 San Sebastián-Donostia, Spain

[§]IKERBASQUE, Basque Foundation for Science, Maria Diaz de Haro 3, 48013 Bilbao, Spain

[∥]Departamento de Física Teórica de la Materia Condensada and Condensed Matter Physics Center (IFIMAC), Universidad Autónoma de Madrid, E-28049 Madrid, Spain

Supporting Information

ABSTRACT: As the size of a molecular emitter becomes comparable to the dimensions of a nearby optical resonator, the standard approach that considers the emitter to be a point-like dipole breaks down. By adoption of a quantum description of the electronic transitions of organic molecular emitters, coupled to a plasmonic electromagnetic field, we are able to accurately calculate the position-dependent coupling strength between a plasmon and an emitter. The spatial distribution of excitonic and photonic quantum states is found to be a key aspect in determining the dynamics of molecular emission in ultrasmall cavities both in the weak and strong coupling regimes. Moreover, we show that the extreme localization of plasmonic fields leads to the selection rule breaking of molecular excitations.

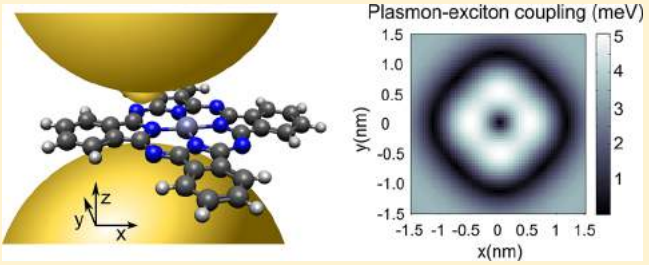

KEYWORDS: *Plasmon−exciton coupling, quantum chemistry, quantum nano-optics, point-dipole approximation, nanoplasmonics, single-molecule spectroscopy*

The strength of the coupling between molecular electronic excitations and cavity optical modes is a magnitude of paramount importance that determines the dynamical properties of important phenomena such as molecular radiative and nonradiative decays (Purcell factors),[1−7] light-matter strong coupling,[8−18] and other coherent quantum optical processes.[19−24] The coupling strength between an emitter and an optical cavity is often estimated as a product of the local electromagnetic field in the optical cavity, $\mathbf{E}_{loc}$, and the dipole moment, $\mathbf{p}_{eg}$, of the emitter's optically allowed electronic transition, as $\hbar g \approx -\mathbf{p}_{eg} \cdot \mathbf{E}_{loc}$, with $\hbar$, the Planck's constant. This coupling is enhanced when the optical cavity mode shows a large quality factor or a small effective mode volume and/or when the electronic transition of the emitter possess a large dipole moment. In this context, the molecular emitter is often considered to be a point-like dipole, since the dimensions of a typical optical cavity and thus the extension of its optical modes are usually orders of magnitude larger than the size of the emitter. However, nanoscale plasmonic resonators result in a class of optical cavities that allow for light localization into deeply subwavelength dimensions, thus reaching effective mode volumes as small as a few nm^3. Under these conditions, emitters such as quantum dots[25−35] and organic molecules[36−41] cannot be described as point-like objects any more, since the spatial extent of their electronic transition densities are of the order of the size of the strongly inhomogeneous local fields of the plasmonic resonator.[7]

In this Letter, we present a quantum theoretical framework that allows us to calculate the coupling between strongly confined plasmonic modes and molecular electronic excitations of spatially extended molecules, identifying the importance of a proper quantum treatment of the molecule to accurately obtain the dynamical properties of the hybrid exciton−plasmon system.[42−44] With the use of two exemplary organic molecules, we reveal the importance of molecular size both in the weak and strong coupling regimes, as well as in the atomic-scale spatial mapping of the coupling strength.

The quantum treatment of the plasmon−exciton coupling presented here combines the canonical quantization of plasmons in metallic particles with quantum chemistry calculations of molecular excitations based on the time-dependent density functional theory (TDDFT) [quantization scheme depicted in Figure 1a]. Plasmon modes are treated as excitations of an incompressible gas of free electrons

Received: December 17, 2017
Revised: February 25, 2018
Published: March 9, 2018

DOI: 10.1021/acs.nanolett.7b05297
Nano Lett. 2018, 18, 2358−2364

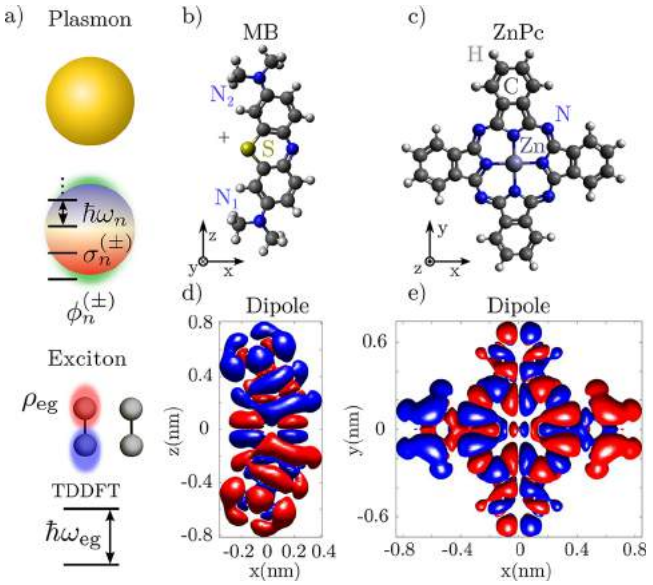

Figure 1. (a) Schematics of the plasmonic resonator−emitter system. The n^{th} plasmonic mode is described as a harmonic oscillation of an incompressible electron gas. Molecular excitations are addressed as two-level systems of energy $\hbar\omega_{eg}$. The plasmon interacts with the molecular transition density ρ_{eg}. (b, c) Atomic structure of (b) methylene blue (MB) and (c) zinc phtalocyanine (ZnPc). (d, e) Isosurface plots of the transition densities (MB, ZnPc) corresponding to the transition between the ground and the singlet excited state calculated within the TDDFT framework (blue, negative values of the density; red, positive ones).

characterized by an electron density, N, and effective electron mass, m_e.[13,24,45−49] Its local dielectric response is given by the standard Drude model as $\varepsilon(\omega) = 1 - \frac{\omega_p^2}{\omega^2 + i\kappa\omega}$, with $\omega_p = \sqrt{\frac{Ne^2}{\varepsilon_0 m_e}}$ as the plasma frequency, e as the electron charge, κ as the metal intrinsic damping, and ε_0 as the vacuum permittivity. Each n^{th} plasmonic mode of frequency ω_n is characterized by its quantized electric potential $\phi_n^{(\pm)}$ and surface charge density $\sigma_n^{(\pm)}$, obtained from the canonical quantization of the electrostatic surface modes, with the superscripts $(\pm)$ marking the positive and negative frequency part. More details are given in the Supporting Information. The plasmonic system can be consequently described by the standard Hamiltonian that resembles a collection of noninteracting harmonic oscillators $H_{pl} = \sum_n \hbar\omega_n \hat{a}_n^\dagger \hat{a}_n$, where $\hat{a}_n$ ($\hat{a}_n^\dagger$) is the bosonic annihilation (creation) operators of the n^{th} plasmonic mode. This framework can be extended to include a nonlocal description of the quantization of the plasmonic modes;[50,51] however, the use of a local classical description can serve to effectively describe the inhomogeneous screened fields in many representative plasmonic cavities,[52−55] as those considered here.

As a counterpart to the plasmon modes, we consider the molecular excitations (excitons) using linear-response TDDFT at the level of the Tamm−Dancoff approximation in vacuum (see Supporting Information). From TDDFT calculations, we obtain the spatial distribution of the oscillating electric charge over the molecule (position $\mathbf{r}$-dependent), which allows us to obtain the transition density, $\rho_{eg}(\mathbf{r})$, formally defined as the expectation value of the electronic density operator $\hat{\rho}(\mathbf{r})$ ($\rho_{eg}(\mathbf{r}) = e\langle e|\hat{\rho}(\mathbf{r})|g\rangle$), accounting for the electronic transitions between the ground $|g\rangle$ and the excited $|e\rangle$ states. Throughout this Letter we consider that the plasmons interact with molecules that are physisorbed or physically separated from the surface of the metallic particles by a dielectric spacer and thus neglect the orbital overlap between the molecular and metal wave functions.

Within this quantum framework, the coupling g_n between the molecular exciton and the n^{th} plasmonic mode is calculated as an integral of its associated potential and the molecular transition density (considering here that the transition density is real):

$$\hbar g_n = \int_{V_{mol}} \rho_{eg}(\mathbf{r})\phi_n^{(+)}(\mathbf{r})\mathrm{d}^3\mathbf{r} \tag{1}$$

where the integral is taken over the molecular volume, V_{mol}. The Hamiltonian describing the plasmon−exciton interaction is $H_{pl-mol} = \hbar\sum_{i,n}[g_{n,i}^* \hat{a}_n^\dagger |g\rangle\langle e_i| + g_{n,i}\hat{a}_n |e_i\rangle\langle g|]$, where $|g\rangle$ ($|e_i\rangle$) is the electronic ground state (excited state i). The interaction Hamiltonian is derived in the rotating wave approximation (RWA), which is valid if the coupling rate is smaller than the excitonic frequency [small Bloch−Siegert shift[56,57] $\sim (g^2/\omega_{eg}) \ll \omega_{eg}$] and if the detuning between the plasmon and the exciton frequency is not too large.

We illustrate the importance of the quantum treatment of the molecular electronic transitions in two specific cases of dye molecules: methylene blue (MB) [Figure 1b] and zinc phtalocyanine (ZnPc) [Figure 1c], due to their relevance in experimental situations.[12,36,37] MB is a molecule with an electronic transition S_z of a strong dipole transition moment (optically active) oriented along the z axis, $p_z = 0.23$ e·nm [axes marked in Figure 1b,c]. ZnPc is a flat molecule with all of the atoms lying on the xy plane, showing two degenerate optically active transitions, S_x and S_y, on the same plane, with a transition dipole moment $p_{x,y} = 0.17$ e·nm. The transition charge densities of the molecular excitons are shown as isosurface plots in Figure 1d,e for the S_z transition of MB (d) and the transition S_x of ZnPc (e), respectively. The positive (red) and negative (blue) transition charge densities are clearly observable at opposite sides of both molecules, corroborating the dipole character of the transitions, continuously distributed over the entire extent of the molecules (~2 nm).

We now apply the hybrid quantization scheme to explore the role of the finite size of the molecule and calculate the dynamics of the population of the excited electronic state $|c_e(t)|^2$ by solving the integro-differential equation for the amplitude, $c_e(t)$, based on the Wigner−Weisskopf approach:[15,58]

$$\dot{c}_e(t) = -\int_0^t \int_{-\infty}^{\infty} J(s) e^{i(\omega_{eg}-s)(t-\tau)} c_e(\tau)\mathrm{d}s\mathrm{d}\tau \tag{2}$$

where $J(s)$ is the spectral density characterizing the coupling of the molecule with the plasmonic system:

$$J(s) = \frac{\kappa}{2\pi}\sum_n \frac{|g_n|^2}{(\omega_n - s)^2 + \left(\frac{\kappa}{2}\right)^2} \tag{3}$$

with ω_n being the frequency of n^{th} plasmonic mode and $\hbar\omega_{eg} = 2.3$ eV (2.8 eV) is the excitation frequency of the ZnPc (MB) molecule. For convenience, we consider that the plasmon decay is proportional to the plasma frequency, $\kappa = 0.01\ \omega_p$. In practice, κ phenomenologically accounts for the intrinsic losses in the metal and can be estimated from the classical dielectric function of the particle material.[59] We have also performed a

DOI: 10.1021/acs.nanolett.7b05297
Nano Lett. 2018, 18, 2358−2364

set of calculations of the system dynamics involving larger values of κ (accounting for larger losses of conventional plasmonic materials) to test its influence on the results presented in this Letter (see Supporting Information). Large values of κ affect the coherence of the dynamics; however, the general trends of the results presented here are valid. Note that in eq 2 we are neglecting the extremely slow intrinsic molecular decay. We solve eq 2 for the initial condition $|c_e(0)|^2 = 1$, thus treating the decay of the initially fully excited molecular exciton. Details of the mathematical solution of this so-called Wigner–Weisskopf problem are provided in the Supporting Information.

We first consider the MB molecule [Figure 1b,d] oriented perpendicularly to the surface of a spherical metal nanoparticle of radius $R = 5$ nm. We plot in Figure 2a,b the spectral density

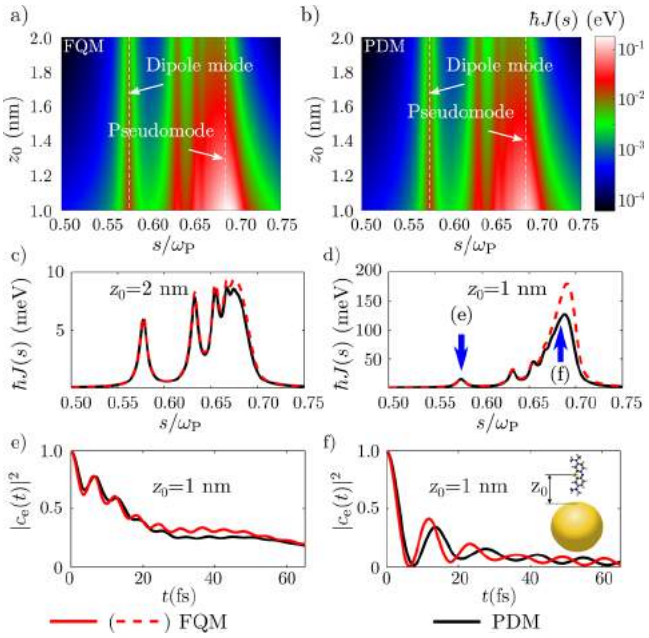

Figure 2. Dynamics of the MB molecular exciton in the proximity of a spherical plasmonic resonator. (a, b) Spectral densities calculated with the FQM (a) and with the PDM (b), as a function of the distance z_0 of the center of the molecule to the particle's surface (radius $R = 5$ nm). (c,d) Spectral densities extracted from parts a and b, for $z_0 = 1$ nm (c) and for $z_0 = 2$ nm (d). (e, f) Selected decay dynamics for the exciton resonant with the dipolar plasmon (e) and to the pseudomode (f) for a separation distance of $z_0 = 1$ nm, as marked in part d. FQM results are displayed with red lines and PDM results with black ones.

as a function of the distance, z_0, between the center of the molecule and the particle's surface. We compare the spectral density obtained using the full quantum model (FQM) in which the transition density is obtained within the TDDFT [Figure 2a], with that obtained with the use of the simplified point-dipole model (PDM) to describe the molecule [Figure 2b]. The same color scale is used for a straightforward comparison. For a more quantitative comparison, in Figure 2c,d, we extract the spectral densities for the smallest $z_0 = 1$ nm (c) and largest $z_0 = 2$ nm (d) within the PDM (black lines) and FQM (red lines). The spectral density maps calculated within both models feature the same qualitative behavior, showing several peaks starting at the frequency of the dipole mode of the sphere (the Fröhlich frequency $\omega_{dip} = \omega_p/\sqrt{3}$) and continuing with a number of higher order modes that build up a strong resonance at around the frequency of the surface plasmon, $\omega_{ps} \approx \omega_p/\sqrt{2}$, the so-called pseudomode.[14]

One of the most striking effects of considering the spatial distribution of the transition density is revealed in the dynamics of the exciton decay, $|c_e(t)|^2$. We analyze in Figure 2e this situation when the MB exciton is resonant with the dipolar plasmon and in Figure 2f when it is resonant with the plasmonic pseudomode. In both cases, the molecule is placed at $z_0 = 1$ nm. When the exciton is resonant with the dipolar mode, the spectral densities, $J(s)$, of the FQM and the PDM are almost identical in the spectral region close to the exciton resonance, thus leading to similar qualitative and quantitative features of the corresponding decay dynamics within both models. In the first stages of the decay, the exciton population shows fast but shallow oscillations that modulate the overall slower nonexponential decay process driven by low-order plasmonic modes. We have checked that the fast dynamics arises mainly due to presence of the pseudomode peak in $J(s)$, despite its large spectral detuning from the exciton frequency. A different picture can be observed in Figure 2f when the pseudomode frequency coincides with the excitonic frequency, $\omega_{ps} \approx \omega_{eg}$. In this case, the decay dynamics feature a clear coherent exchange of the exciton population with the plasmonic pseudomode. In this strong coupling regime, we find that the spectral density is larger in the FQM than in the PDM [Figure 2d], resulting in about ≈20% faster vacuum Rabi oscillations due to the proximity of one side of the molecule to the metallic surface. Notice that the coupling of the molecular exciton to the pseudomode is much more sensitive spatially than in the dipolar case due to the extremely localized character of the pseudomode.

We also consider an alternative situation of coupling by analyzing the exciton dynamics of a transition of the ZnPc molecule, which is oriented horizontally with respect to the metal nanoparticle. The spectral densities obtained from the two approaches are shown in Figure 3a,b, using the same color

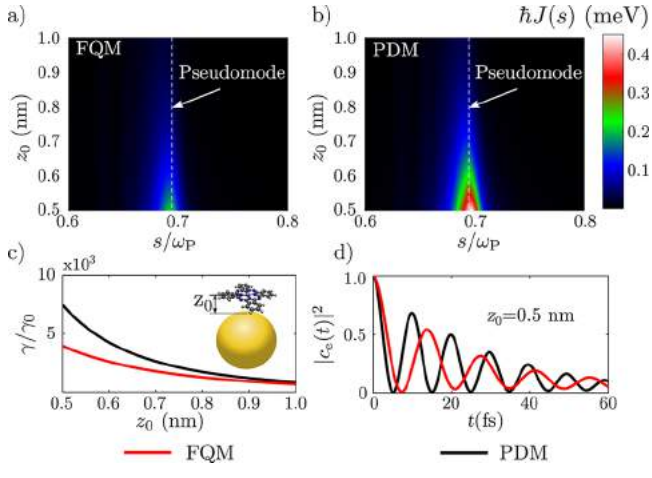

Figure 3. Dynamics of the ZnPc molecular exciton near a spherical plasmonic resonator. (a, b) Spectral densities as a function of the distance of the molecule to the particle's surface z_0 [see inset in part c] within the FQM (a) and within the PDM (b). (c) Plasmonic enhancement of the total decay rate as a function of z_0, when the plasmon resonance is strongly blue-detuned from the molecular exciton. (d) Dynamics of the exciton for $z_0 = 0.5$ nm when the exciton frequency corresponds to the pseudomode peak. The red line corresponds to the FQM and the black line to the PDM.

DOI: 10.1021/acs.nanolett.7b05297
Nano Lett. 2018, 18, 2358–2364

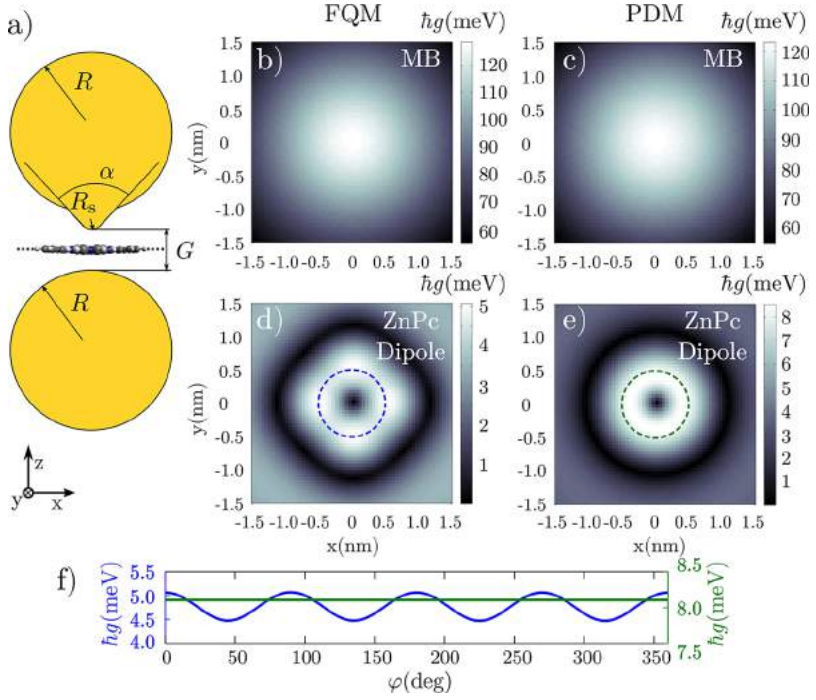

Figure 4. (a) Schematics of the geometry used to map the coupling strength. A plasmonic dimer of radii R = 5 nm with a protrusion of R_s = 0.2 nm (cone opening angle α = 72.5°) hosts a molecule located at a position (x, y, z = 0) within the gap of width G. MB (G = 2 nm) and ZnPc (G = 1 nm) molecules are considered. (b−e) Maps of the coupling constant $g(\mathbf{r}_0)$ between the plasmon dipolar gap mode and the molecular electronic transition as a function of the lateral displacement of the center of the molecule around the gap (center of the gap at $x = y = 0$). (b, c) Maps of g calculated for a vertically oriented MB molecule. (d, e) Maps of effective g for a horizontally positioned ZnPc molecule, which considers both lowest energy degenerated dipole transitions. Maps to the left obtained within the FQM, and maps to the right within the PDM. (f) Circular cut of g at a distance of 0.5 nm from the center as indicated with dashed lines in parts d and e. FQM (blue) and PDM (green) are compared.

scale in both cases. Both the FQM and the PDM exhibit a single peak at the pseudomode frequency. However, as opposite to the MB case, the amplitude of this peak is substantially reduced in the FQM with respect to that obtained within PDM. This occurs because the higher order plasmon modes show a high spatial modulation, which exceeds that of the transition density, thus softening the plasmon−exciton interaction. For analyzing the dynamics, we first focus on a situation where the exciton weakly interacts with a far blue-detuned plasmonic resonance. We select this detuned case by assuming a value of the plasma frequency ($\hbar\omega_p \approx 9$ eV), which locates the frequency of the pseudomode ($\hbar\omega_{ps} \approx 6.4$ eV) far away from the ZnPc exciton ($\hbar\omega_{eg} = 2.3$ eV). We checked that the RWA also describes correctly the dynamics under these conditions. In this case, the molecule is weakly coupled to the plasmonic excitations, so that the exciton decays exponentially, $|c_e(t)|^2 = e^{-\gamma t}$ (Purcell effect). The decay rate γ can be related to the spectral function of the plasmons as $\gamma = 2\pi J(\omega_{eg})$ (see Supporting Information), which for the PDM reduces to the well-known expression $\gamma = \frac{2\omega_{eg}^2}{c^2\varepsilon_0}[\mathbf{p}_{eg}\cdot\Im\{\mathbf{G}(\mathbf{r}_0, \mathbf{r}_0)\}\cdot\mathbf{p}_{eg}]$ (with c as the speed of light in a vacuum)[60] involving the imaginary part ($\Im\{\cdot\}$) of the (quasi-static) electric dyadic Green's function $\mathbf{G}(\mathbf{r}_0, \mathbf{r}_0)$ evaluated at position $\mathbf{r}_0$ of the dipolar emitter.

In Figure 3c, we show the dependence of the plasmon-induced decay rate, γ, normalized to the vacuum decay of the transition, γ_0, as a function of the distance of the molecule (the central Zn atom) to the surface of the metal nanoparticle, as calculated with the FQM (red lines) and with the PDM (black lines). The values of the decay rate enhancement γ/γ_0 (the Purcell factor) reach almost up to 10^4 for the closest separation distance (z_0 = 0.5 nm) when a point-like dipole is considered. At this distance, the decay rate calculated with the quantum model, dominated by the interaction with the pseudomode, is reduced by a factor of around 2 with respect to the PDM result. When the distance from the surface increases, the values of the decay rate from both models become closer, recovering the limit of the point-dipole approximation from distances of approximately $z_0 \approx 1$ nm. In a second scenario, we make the pseudomode frequency to coincide with the molecular exciton, $\omega_{ps} \approx \omega_{eg}$, also for a distance of z_0 = 0.5 nm. Under these conditions, the plasmon−exciton coupling is strong and the calculated dynamics of the excited state, $|c_e(t)|^2$, results in clear Rabi oscillations [Figure 3d]. The comparison of the dynamics obtained from the FQM (red lines) with that of the PDM (black lines) yields quantitative differences in the period of the Rabi oscillations, around 40% smaller in the PDM than in the FQM.

So far our results demonstrate that it is necessary to use a full quantum description of the molecular size effect of an exciton in order to describe quantitatively its interaction with plasmonic cavities whose associated electromagnetic fields are localized at the nanometer scale. In some cases, the point-dipole approach overestimates the coupling (like in the ZnPc case), whereas in others the exciton−plasmon interaction is considerably larger than that predicted by the PDM (as in the case of the MB molecule). Moreover, in many realistic plasmonic cavities, near-field localization can be achieved by means of complex morphologies such as protrusions emerging on the facets in gaps, which lead to extreme field localization at the atomic scale.[61] A similar effect can also be obtained, for instance, in the gap between a metallic substrate and an atomically sharp tip of

DOI: 10.1021/acs.nanolett.7b05297
Nano Lett. 2018, 18, 2358−2364

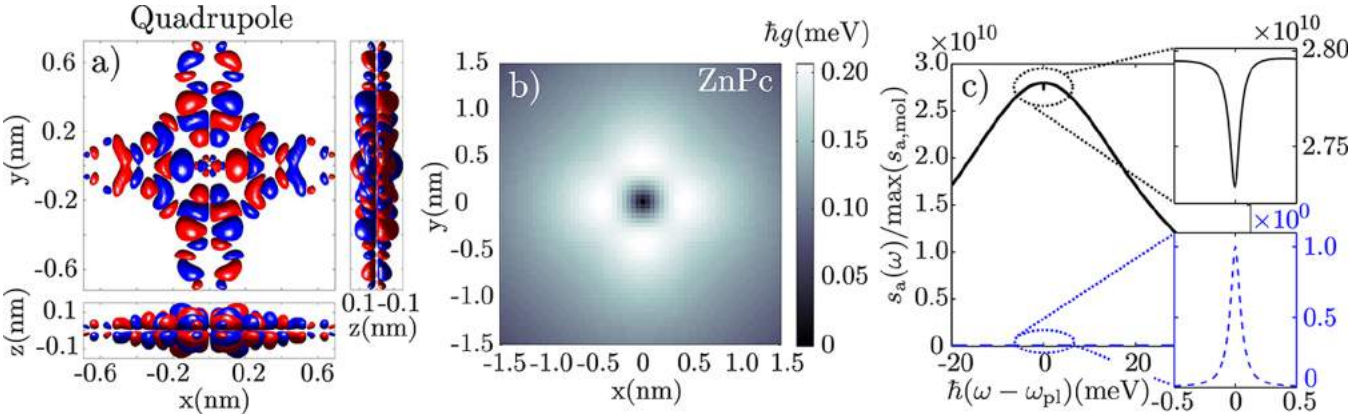

Figure 5. Breaking of optical selection rules for the quadrupolar transition of ZnPc. (a) Isosurface plot of the transition charge density produced by the quadrupolar electronic transition of the ZnPc molecule. The positive values are red, and the negative values are blue. (b) Map of the plasmon−exciton effective coupling constant $g^{ZnPc}_{S_{xz(yz)}}$, as the plasmonic cavity [depicted in Figure 4a] is scanned across the molecule in the *xy* plane. (c) Absorption spectra of the plasmonic cavity with the molecule inside (black line) and of the bare molecule in a vacuum (blue-dashed line). The broadening of the molecular dark (dk) exciton is considered to be $\hbar\gamma_{dk}$ = 0.1 meV. The spectra are normalized to the maximum of the bare-molecule absorption, $s_a(\omega)/\max(s_{a,mol})$, and centered with respect to the frequency of the bonding dipolar plasmon ω_{pl} of the cavity. The absorption spectrum of the coupled molecule−cavity system features a Fano-like dip that results from the plasmon−molecule interaction and therefore serves as an experimental signal contrast. The absorption spectrum of the bare molecule in a vacuum has a form of a Lorentzian peak of ≈9 orders of magnitude smaller amplitude compared to the depth of the Fano-like dip.

a scanning probe microscope.[36−38,40,41,62,63] The latter situation allows us to optically map the magnitude of plasmon−exciton coupling, as the sharp tip is scanned over the molecule. We reproduce this situation in a plasmonic dimer with an atomistic protrusion in the gap, whose geometry is depicted in Figure 4a. Such model is able to quantitatively reproduce the near-field distribution around atomic-scale features in plasmonic cavities, as recently validated by comparison with the TDDFT results.[55] In the following, we always choose a plasma frequency such that the lowest-energy gap plasmon is resonant with the exciton of the molecule and calculate the coupling strength between the two as the gap is scanned over the molecule in the horizontal plane *xy*, keeping *z* constant.

We first place into the gap the MB molecule oriented vertically (electronic transistion S_z), and compare the map of the coupling strength, calculated within the FQM [Figure 4b] with that obtained with the PDM [Figure 4c]. The coupling is maximized when the molecule is positioned at the center of the gap and reaches values of up to 120 meV, being larger in the FQM by ≈10 meV than in the PDM. The magnitude of the coupling decreases as the molecule is displaced off the center, following the decay of the electric field component along the dimer axis. The point-dipole approximation [Figure 4c] in this case reproduces well both the qualitative and quantitative features of the first-principles calculation [Figure 4b], validating the use of this approach in this highly symmetric situation.

A more dramatic situation occurs when the ZnPc molecule is considered (with the plane of the molecule perpendicular to the dimer axis). As ZnPc has two degenerate transitions, S_x and S_y, we calculate the map of the effective coupling $(g^{ZnPc}_{S_{x(y)}}(\mathbf{r}_0) = \{|g^{ZnPc}_{S_x}(\mathbf{r}_0)|^2 + |g^{ZnPc}_{S_y}(\mathbf{r}_0)|^2\}^{1/2})$ [Figure 4d,e] with the FQM (d) and with the PDM (e). When the molecule is placed at the center of the cavity, both maps exhibit a minimum (zero) originated by the vanishing overlap integral between a rotationally symmetrical plasmon mode and a horizontal electronic dipolar transition in the molecule. Away from the center, the C_{4v} symmetry is broken and the map shows a doughnut-like shape, following the pattern of the radial component of the electric local field in the proximity of the atomistic protrusion.[39,61,62] Interestingly, whereas the result of the PDM [Figure 4e] is fully rotationally symmetric, the FQM map [Figure 4d] acquires the 4-fold symmetry of the molecular sample (D_{4h}). We highlight this effect by plotting in Figure 4f a cut along the circular trajectory marked by the blue circle in Figure 4d and the green circle in Figure 4e. The FQM result exhibits experimentally accessible oscillations of the coupling constant, characterized by ≈10% variation, whereas the PDM yields a constant profile. Importantly, the FQM yields a coupling constant reaching roughly one-half of the coupling strength obtained from the PDM. These values are fully consistent with the experimental ones reported for this kind of system.[40,41]

The effect of the extreme field localization in plasmonic cavities can also have a dramatic impact on the optical selection rules governing the interaction of the incident light with the molecular transitions. To demonstrate this, we calculate the charge transition densities of a degenerate quadrupolar electronic transition S_{xz} (S_{yz}) of ZnPc (quadrupolar moment $Q_{yz} = Q_{xz} = \int xz\rho_{S_{xz}}d^3\mathbf{r} \approx 2.74 \times 10^{-4}$ e·nm^2 and energy $\hbar\omega_{dk}$ ≈ 2.97 eV), which does not carry any dipole moment and is thus effectively dark (dk) for an incident plane wave in a vacuum. We show the corresponding transition density $\rho_{S_{xz}}$ in Figure 5a. Following the same procedure as for the degenerate dipole transitions S_x and S_y, we calculate the spatial map of the effective coupling constant $g^{ZnPc}_{Sxz(yz)} = \{|g^{ZnPc}_{Sxz}|^2 + |g^{ZnPc}_{yz}|^2\}^{1/2}$ between the quadrupolar excitonic transitions and the same bonding dipolar plasmon as in the dimer structure of Figure 4a. The map of $g^{ZnPc}_{S_{xz(yz)}}$ is shown in Figure 5b. The spatial distribution of $g^{ZnPc}_{S_{xz(yz)}}$ exhibits a 4-fold symmetry, D_{4h}, as was also found for the dipolar transition. The maximum value of the plasmon−exciton coupling obtained for this situation reaches ≈0.2 meV, which sets the interaction into the weak coupling regime. Nevertheless, the calculated value of $g^{ZnPc}_{S_{xz(yz)}}$ is large enough to allow for detection of the originally dark excitonic transition in the plasmon-enhanced absorption spectrum.

DOI: 10.1021/acs.nanolett.7b05297
Nano Lett. 2018, 18, 2358−2364

To demonstrate this breaking of optical selection rules, we consider the values of $g^{ZnPc}_{S_{xz(yz)}}$ obtained for a position of the molecule in the atomically sharp plasmonic gap at x = 0.4 nm and y = 0 nm and calculate the optical absorption spectra,[64−66] $s_a(\omega)$, of the coupled system. For this calculation, we assume that the intrinsic width of the molecular transition is $\hbar\gamma_{dk}$ = 0.1 meV, taken as a representative intermediate value of fluorescent molecules. The actual value of γ_{dk} will determine the magnitude of the absorption dip (see Supporting Information). In Figure 5c, we compare the spectrum of the coupled molecule−cavity system (black line) with the absorption of the molecule in a vacuum (blue-dashed line). The spectra are normalized to the maximal value of the bare-molecule absorption $s_{a,mol}(\omega)$. In the calculation, we assume that the incident electromagnetic wave is polarized along the axis of the plasmonic dimer and therefore effectively couples mainly to the bonding dimer plasmon. Further details of the calculation are provided in the Supporting Information. The spectrum of the cavity-molecule system shows the shape of a broad Lorentzian resonance originated from light absorbed by the bonding dimer plasmon perturbed by a small spectral dip that emerges due to the ZnPc quadrupolar electronic transition (Fano-like profile). On the other hand, the absorption peak of the bare molecule in a vacuum cannot be resolved on the selected scale and the blue-dashed line appears to be flat. In the inset of Figure 5c, we therefore zoom in on the molecular absorption features and compare their relative spectral intensities. Strikingly, the size of the absorption dip obtained in the plasmonic cavity is ≈9 orders of magnitude larger than the absorption peak of the bare molecule, thus making the quadrupolar excitonic transition accessible to optical absorption spectroscopy.

Finally, it is worthwhile to note that in practical experiments concerning molecules in atomically sharp plasmonic cavities, as those considered here, there might be additional effects that would require more sophisticated treatments of the metal-molecule interface regarding both the electronic structure as well as the electromagnetic interaction. The extreme localization in plasmonic cavities often relies on atomic-scale corrugations at the metal-nanoparticle surface which have been shown to vary along time due to thermal diffusion of the metallic surface atoms.[39] Low temperature experiments are thus required under certain circumstances to stabilize the particle morphology. Additionally, the ground-state geometry as well as the energies of the molecular excitons will be influenced by screening effects of the nearby metallic surfaces and, in the case of experiments performed in air or solvent, also of the wetting layer present in the plasmonic gap. These effects will generally modify the quantum-chemical properties of the molecules and require more complex ab initio modeling. Nevertheless, the first-principles approach presented in this Letter provides a good qualitative and quantitative picture of the coupling between plasmons and single-molecular excitations under well-controlled conditions.[12,40,41]

In conclusion, we have shown the importance of considering the full spatial extent of molecular electronic transitions to describe the plasmon−exciton coupling at the nanometric and subnanometric scales. This coupling strength stems from a delicate balance between the spatial dependence of both the excitonic transition charge density and the photonic fields, and therefore, only a quantum model that fully incorporates the inhomogeneities of the exciton transition charge density can describe quantitatively this interplay. By using a first-principles methodology to describe the quantum chemistry of organic molecules placed inside optical resonators, we have revealed the limitations of the point-dipole approach to address the exciton dynamics both in weak and strong coupling regimes. We have found that each situation requires a detailed analysis as in some occasions the point-dipole approximation overestimates the coupling, whereas it underestimates its strength in others. We have further explored the possibility to optically map the plasmon−exciton coupling strength of a molecule placed into an atomically sharp cavity and obtained values nicely corresponding with experimental results reported in the literature.[12,40,41] Furthermore, we have shown that this type of cavity is able to produce optical-selection-rule breaking of molecular excitations. Our findings are of importance in nanoscale optical spectroscopy, in setting optical paths to engineer chemical reactivity at the single-molecule level, as well as in coherent control of the nanoscale light-matter interaction.

■ ASSOCIATED CONTENT

Supporting Information

The Supporting Information is available free of charge on the ACS Publications website at DOI: 10.1021/acs.nanolett.7b05297.

Technical details about the canonical quantization of plasmons and calculation of the plasmon−exciton coupling in the spherical geometry, the technical implementation of the excitonic time-dynamics, exciton dynamics for different values of plasmon damping, methodology to calculate the absorption spectra, and influence of the molecular width in the absorption spectra (PDF)

■ AUTHOR INFORMATION

Corresponding Author

*E-mail: aizpurua@ehu.eus.

ORCID

Francisco J. García-Vidal: 0000-0003-4354-0982

Javier Aizpurua: 0000-0002-1444-7589

Notes

The authors declare no competing financial interest.

■ ACKNOWLEDGMENTS

J.A., R.E., and T.N. acknowledge the project FIS2016-80174-P from MINECO, project 70NANB15H32 from U.S. Department of Commerce, National Institute of Standards and Technology, and project PI2017-30 of the Department of Education of the Basque Government. F.J.G.-V. acknowledges funding by the European Research Council under Grant Agreement ERC-2011-AdG 290981 and by the Spanish MINECO under contract MAT2014-53432-C5-5-R. D.C. acknowledges project CTQ2016-80955 from MINECO.

■ REFERENCES

(1) Purcell, E. M.; Torrey, H. C.; Pound, R. V. *Phys. Rev.* **1946**, *69*, 37−38.

(2) Gersten, J.; Nitzan, A. *J. Chem. Phys.* **1981**, *75*, 1139−1152.

(3) Itoh, T.; Yamamoto, Y. S.; Ozaki, Y. *Chem. Soc. Rev.* **2017**, *46*, 3904−3921.

(4) Koenderink, A. F. *Opt. Lett.* **2010**, *35*, 4208−4210.

(5) Sauvan, C.; Hugonin, J. P.; Maksymov, I. S.; Lalanne, P. *Phys. Rev. Lett.* **2013**, *110*, 237401.

(6) Kristensen, P. T.; Hughes, S. *ACS Photonics* **2014**, *1*, 2−10.

DOI: 10.1021/acs.nanolett.7b05297
Nano Lett. 2018, 18, 2358−2364

(7) Rivera, N.; Kaminer, I.; Zhen, B.; Joannopoulos, J. D.; Soljačić, M. *Science* **2016**, *353*, 263−269.
(8) Zengin, G.; Wersäll, M.; Nilsson, S.; Antosiewicz, T. J.; Käll, M.; Shegai, T. *Phys. Rev. Lett.* **2015**, *114*, 157401.
(9) Brune, M.; Schmidt-Kaler, F.; Maali, A.; Dreyer, J.; Hagley, E.; Raimond, J.; Haroche, S. *Phys. Rev. Lett.* **1996**, *76*, 1800.
(10) Dintinger, J.; Klein, S.; Bustos, F.; Barnes, W. L.; Ebbesen, T. W. *Phys. Rev. B: Condens. Matter Mater. Phys.* **2005**, *71*, 035424.
(11) Bellessa, J.; Bonnand, C.; Plenet, J. C.; Mugnier, J. *Phys. Rev. Lett.* **2004**, *93*, 036404.
(12) Chikkaraddy, R.; de Nijs, B.; Benz, F.; Barrow, S. J.; Scherman, O. A.; Rosta, E.; Demetriadou, A.; Fox, P.; Hess, O.; Baumberg, J. J. *Nature* **2016**, *535*, 127−130.
(13) Trügler, A.; Hohenester, U. *Phys. Rev. B: Condens. Matter Mater. Phys.* **2008**, *77*, 115403.
(14) Delga, A.; Feist, J.; Bravo-Abad, J.; Garcia-Vidal, F. J. *J. Opt.* **2014**, *16*, 114018.
(15) Li, R.-Q.; Hernángomez-Pérez, D.; García-Vidal, F. J.; Fernández-Domínguez, A. I. *Phys. Rev. Lett.* **2016**, *117*, 107401.
(16) Galego, J.; Garcia-Vidal, F. J.; Feist, J. *Phys. Rev. X* **2015**, *5*, 041022.
(17) Delga, A.; Feist, J.; Bravo-Abad, J.; Garcia-Vidal, F. J. *Phys. Rev. Lett.* **2014**, *112*, 253601.
(18) Törmä, P.; Barnes, W. L. *Rep. Prog. Phys.* **2015**, *78*, 013901.
(19) Tame, M. S.; McEnery, K.; Özdemir, Ş.; Lee, J.; Maier, S.; Kim, M. *Nat. Phys.* **2013**, *9*, 329−340.
(20) Zhu, K.-D.; Li, W.-S. *J. Phys. B: At., Mol. Opt. Phys.* **2001**, *34*, L679−L686.
(21) Miroshnichenko, A. E.; Flach, S.; Kivshar, Y. S. *Rev. Mod. Phys.* **2010**, *82*, 2257−2298.
(22) Yannopapas, V.; Paspalakis, E.; Vitanov, N. V. *Phys. Rev. Lett.* **2009**, *103*, 063602.
(23) Hatef, A.; Singh, M. R. *Phys. Rev. A: At., Mol., Opt. Phys.* **2010**, *81*, 063816.
(24) Bergman, D. J.; Stockman, M. I. *Phys. Rev. Lett.* **2003**, *90*, 027402.
(25) Andersen, M. L.; Stobbe, S.; Sørensen, A. S.; Lodahl, P. *Nat. Phys.* **2011**, *7*, 215−218.
(26) Madsen, K. H.; Ates, S.; Lund-Hansen, T.; Löffler, A.; Reitzenstein, S.; Forchel, A.; Lodahl, P. *Phys. Rev. Lett.* **2011**, *106*, 233601.
(27) Jain, P. K.; Ghosh, D.; Baer, R.; Rabani, E.; Alivisatos, A. P. *Proc. Natl. Acad. Sci. U. S. A.* **2012**, *109*, 8016−8019.
(28) Stobbe, S.; Kristensen, P. T.; Mortensen, J. E.; Hvam, J. M.; Mørk, J.; Lodahl, P. *Phys. Rev. B: Condens. Matter Mater. Phys.* **2012**, *86*, 085304.
(29) Kristensen, P. T.; Mortensen, J. E.; Lodahl, P.; Stobbe, S. *Phys. Rev. B: Condens. Matter Mater. Phys.* **2013**, *88*, 205308.
(30) Gordon, J. M.; Gartstein, Y. N. *J. Opt. Soc. Am. B* **2014**, *31*, 2029−2035.
(31) Pelton, M. *Nat. Photonics* **2015**, *9*, 427−435.
(32) Cotrufo, M.; Fiore, A. *Phys. Rev. B: Condens. Matter Mater. Phys.* **2015**, *92*, 125302.
(33) Tighineanu, P.; Sørensen, A. S.; Stobbe, S.; Lodahl, P. *Phys. Rev. Lett.* **2015**, *114*, 247401.
(34) Lodahl, P.; Mahmoodian, S.; Stobbe, S. *Rev. Mod. Phys.* **2015**, *87*, 347.
(35) Yang, C.-J.; An, J.-H. *Phys. Rev. A: At., Mol., Opt. Phys.* **2016**, *93*, 053803.
(36) Zhang, R.; Zhang, Y.; Dong, Z. C.; Jiang, S.; Zhang, C.; Chen, L. G.; Zhang, L.; Liao, Y.; Aizpurua, J.; Luo, Y.; Yang, J. L.; Hou, J. G. *Nature* **2013**, *498*, 82−86.
(37) Zhang, Y.; Luo, Y.; Zhang, Y.; Yu, Y.-J.; Kuang, Y.-M.; Zhang, L.; Meng, Q.-S.; Luo, Y.; Yang, J.-L.; Dong, Z.-C.; Hou, J. G. *Nature* **2016**, *531*, 623−627.
(38) Doppagne, B.; Chong, M. C.; Lorchat, E.; Berciaud, S.; Romeo, M.; Bulou, H.; Boeglin, A.; Scheurer, F.; Schull, G. *Phys. Rev. Lett.* **2017**, *118*, 127401.
(39) Benz, F.; Schmidt, M. K.; Dreismann, A.; Chikkaraddy, R.; Zhang, Y.; Demetriadou, A.; Carnegie, C.; Ohadi, H.; de Nijs, B.; Esteban, R.; Aizpurua, J.; Baumberg, J. J. *Science* **2016**, *354*, 726−729.
(40) Imada, H.; Miwa, K.; Imai-Imada, M.; Kawahara, S.; Kimura, K.; Kim, Y. *Phys. Rev. Lett.* **2017**, *119*, 013901.
(41) Zhang, Y.; Meng, Q.-S.; Zhang, L.; Luo, Y.; Yu, Y.-J.; Yang, B.; Zhang, Y.; Esteban, R.; Aizpurua, J.; Luo, Y.; Yang, J.-L.; Dong, Z.-C.; Hou, J. G. *Nat. Commun.* **2017**, *8*, 15225.
(42) Litz, J. P.; Brewster, R. P.; Lee, A. B.; Masiello, D. J. *J. Phys. Chem. C* **2013**, *117*, 12249−12257.
(43) Gao, Y.; Neuhauser, D. *J. Chem. Phys.* **2013**, *138*, 181105.
(44) Nascimento, D. R.; DePrince, A. E., III *J. Chem. Phys.* **2015**, *143*, 214104.
(45) Ritchie, R. H. *Phys. Rev.* **1957**, *106*, 874−881.
(46) Nordlander, P.; Oubre, C.; Prodan, E.; Li, K.; Stockman, M. *Nano Lett.* **2004**, *4*, 899−903.
(47) Prodan, E.; Nordlander, P. *J. Chem. Phys.* **2004**, *120*, 5444−5454.
(48) Prodan, E.; Radloff, C.; Halas, N. J.; Nordlander, P. *Science* **2003**, *302*, 419−422.
(49) Hohenester, U.; Trügler, A. *Comput. Phys. Commun.* **2012**, *183*, 370−381.
(50) Ford, G.; Weber, W. *Phys. Rep.* **1984**, *113*, 195−287.
(51) Crowell, J.; Ritchie, R. H. *Phys. Rev.* **1968**, *172*, 436−440.
(52) Teperik, T. V.; Nordlander, P.; Aizpurua, J.; Borisov, A. G. *Phys. Rev. Lett.* **2013**, *110*, 263901.
(53) Luo, Y.; Fernandez-Dominguez, A. I.; Wiener, A.; Maier, S. A.; Pendry, J. B. *Phys. Rev. Lett.* **2013**, *111*, 093901.
(54) Dezfouli, M. K.; Tserkezis, C.; Mortensen, N. A.; Hughes, S. *Optica* **2017**, *4*, 1503−1509.
(55) Urbieta, M.; Barbry, M.; Zhang, Y.; Koval, P.; Sánchez-Portal, D.; Zabala, N.; Aizpurua, J. *ACS Nano* **2018**, *12*, 585−595.
(56) Bloch, F.; Siegert, A. *Phys. Rev.* **1940**, *57*, 522−527.
(57) Shirley, J. H. *Phys. Rev.* **1965**, *138*, B979−B987.
(58) Breuer, H.-P.; Petruccione, F. *The theory of open quantum systems*; Oxford University Press, 2003.
(59) Wang, F.; Shen, Y. R. *Phys. Rev. Lett.* **2006**, *97*, 206806.
(60) Novotny, L.; Hecht, B. *Principles of Nano-Optics*; Cambridge University Press, 2006.
(61) Barbry, M.; Koval, P.; Marchesin, F.; Esteban, R.; Borisov, A. G.; Aizpurua, J.; Sánchez-Portal, D. *Nano Lett.* **2015**, *15*, 3410−3419.
(62) Trautmann, S.; Aizpurua, J.; Götz, I.; Undisz, A.; Dellith, J.; Schneidewind, H.; Rettenmayr, M.; Deckert, V. *Nanoscale* **2017**, *9*, 391−401.
(63) Reecht, G.; Scheurer, F.; Speisser, V.; Dappe, Y. J.; Mathevet, F.; Schull, G. *Phys. Rev. Lett.* **2014**, *112*, 047403.
(64) Bloom, S.; Margenau, H. *Phys. Rev.* **1953**, *90*, 791−794.
(65) Mollow, B. R. *Phys. Rev. A: At., Mol., Opt. Phys.* **1972**, *5*, 2217−2222.
(66) Zhou, P.; Swain, S. *Phys. Rev. Lett.* **1997**, *78*, 832−835.

DOI: 10.1021/acs.nanolett.7b05297
Nano Lett. 2018, 18, 2358−2364